ORIGINAL ARTICLE

Bilayer hydrogel dressing with lysozyme-enhanced photothermal therapy for biofilm eradication and accelerated chronic wound repair

Yizhen Wang[a,†], Qijun Lv[a,†], You Chen[b], Langtao Xu[b], Miao Feng[b], Zhiyong Xiong[a], Jiajun Li[a], Jie Ren[c,*], Jie Liu[b,*], Bo Liu[a,*]

[a]Department of General Surgery, the Third Affiliated Hospital of Sun Yat-sen University, Guangzhou 510630, China
[b]School of Biomedical Engineering, Sun Yat-sen University, Guangzhou 510006, China
[c]Department of Ultrasound, the Third Affiliated Hospital of Sun Yat-sen University, Guangzhou 510630, China

Abstract   Biofilms are closely associated with the tough healing and dysfunctional inflammation of chronic wounds. Photothermal therapy (PTT) emerged as a suitable alternative which could destroy the structure of biofilms with local physical heat. However, the efficacy of PTT is limited because the excessive hyperthermia could damage surrounding tissues. Besides, the difficult reserve and delivery of photothermal agents makes PTT hard to eradicate biofilms as expectation. Herein, we present a GelMA-EGF/Gelatin-MPDA-LZM bilayer hydrogel dressing to perform lysozyme-enhanced PTT for biofilms eradication and a further acceleration to the repair of chronic wounds. Gelatin was used as inner layer hydrogel to reserve lysozyme (LZM) loaded mesoporous polydopamine (MPDA) (MPDA-LZM) nanoparticles, which could rapidly liquefy while temperature rising so as to achieve a bulk release of nanoparticles. MPDA-LZM nanoparticles serve as photothermal agents with antibacterial capability, could deeply penetrate and destroy biofilms. In addition, the outer layer hydrogel consisted of gelatin methacryloyl (GelMA) and epidermal growth factor (EGF) promoted wound healing and tissue regeneration. It displayed remarkable efficacy on alleviating infection and accelerating wound healing *in vivo*. Overall, the innovative therapeutic strategy we came up with has significant effect on biofilms eradication and shows promising application in promoting the repair of clinical chronic wounds.

*Corresponding authors. Tel./fax: +86 20 82179243 (Jie Ren); +86 20 39332145 (Jie Liu); +86 20 82179742 (Bo Liu).
    E-mail addresses: renj@mail.sysu.edu.cn (Jie Ren), liujie56@mail.sysu.edu.cn (Jie Liu), liubo3@mail.sysu.edu.cn (Bo Liu).
    †These authors made equal contributions to this work.

1. Introduction

Chronic wounds are considered a major healthcare problem all over the world. Common types of chronic wounds like diabetic foot ulcers, pressure sores, venous ulcers, and surgical site infection usually represent a stuck or delayed condition of healing process of wounds[1,2]. The nonhealing wounds could cause persistent infection or pain, prolong hospital stays, even lead to amputation or severe complications like sepsis[3]. It is common that such nonhealing wounds are often relate to persistent infection and the formation of biofilms[4]. Studies show that biofilms are contained in more than 60% of chronic wounds infection[3,5,6]. It could aggravate the dysfunctional inflammation of chronic wounds and lead to a more difficult circumstance of healing[2,7]. When bacterial infection happens in wound site, bacteria tend to aggregate as a community and embedded in extracellular polymeric substances (EPS) produced by themselves, constitute a compact structure called biofilms[8,9]. EPS matrix could act as a firm physical barrier that protects bacteria from the attack of antibacterial agents and host immune responses, thus making the bacteria become drug-resistant[3,9]. Normal antibacterial agents such as antibiotics, bactericidal enzymes, antimicrobial peptides, or quaternary ammonium compounds could not exert effective antibacterial ability because biofilms restrict the penetration of drugs[10]. The existence of biofilms severely hinders the treatment of infection, result in inflammatory dysregulation. Therefore, eliminating biofilms is necessary for accelerating the healing of chronic wounds. In consideration of the insensitive to chemotherapy, mechanical or surgical removal of biofilms is the most common approach in clinical treatment[8]. However, this approach will bring inevitable destruction to surrounding tissues apart from wound area. Besides, biofilms recur easily even after the treatment. Given all this, the exploration of efficient ways to eradicate biofilms is extremely needed.

Recently, photothermal therapy and photodynamic therapy have been studied to treat chronic wounds with biofilms[11−14]. Photothermal therapy (PTT) based on photothermal agents could destroy the structure and components of biofilms by physical heat generated under near-infrared (NIR) light irradiation[15]. Metal-based nanocomposites[11,16,17], graphene-based nanoplatforms[18], and polydopamine (PDA) nanocomposites were exploited as great photothermal agents candidates to generate enough thermal effect to eliminate biofilms[19−22]. Especially, photothermal agents like nanoparticles could exhibit better penetration of biofilm due to the appropriate size to get through water channels and EPS[14,23,24], indicating their better elimination efficiency within controllable temperature range. However, the biofilm elimination efficacy of PTT is still unsatisfactory while the local temperature rise must be controlled within a safe range in case of hurting the surrounding normal tissues[25]. It is difficult to entirely eradicate biofilms with a relative low temperature PTT. Thus some approaches should be developed to enhance the efficacy of PTT on biofilm eradication. Furthermore, how to reserve and continuously delivery photothermal agents to wounds at any positions are challenges remaining. To solve these problems, nanocarrier-loaded biomaterials dressing for locally drug delivery has been explored[26−29]. Saleh et al.[30] demonstrated a nanoparticle-laden adhesive hydrogel which could convey miRNA to accelerate wound healing. Li et al.[26] reported silica-based nanocomposites hydrogel scaffolds that possessed antibacterial capability for promoting diabetic wound repair. Therefore, it is meaningful to seek a potent way to combine PTT with biomaterials dressing to effectively eradicate biofilms and promote the repair of chronic wounds comprehensively.

Herein, our group developed an original GelMA/gelatin-based bilayer hydrogel dressing containing EGF and lysozyme-loaded mesoporous polydopamine (MPDA) nanoparticles to achieve enhanced photothermal therapy and accelerated repair for severe infected chronic wounds with biofilms (see Scheme 1). MPDA nanoparticles possess outstanding photothermal conversion capability as well as excellent biocompatibility[25,31]. More importantly, the mesoporous structure of MPDA nanoparticles provides large specific surface area, which makes them available for more efficient drug loading and delivery[32]. So that we can acquire an enhanced photothermal effect by loading plenty of antibacterial agents on MPDA nanoparticles to cover the deficiency of low temperature PTT. Lysozyme (LZM) is a bactericidal enzyme that naturally exists in mammalian secretions[33,34]. As the component of immune system, it could kill bacteria by specifically hydrolyze the peptidoglycan in bacterial cell wall, thus resisting bacterial infection[35,36]. It has been wildly used in eye drops or wound healing creams to exert antibacterial activity[37]. In this study, we used MPDA nanoparticles loading lysozyme (i.e., MPDA-LZM nanoparticles) to eradicate biofilms synergistically. Photothermal effect performed by MPDA nanoparticles could destroy the structure of biofilms so that the loaded LZM could penetrate deeply into biofilms and kill the bacteria underneath. Furthermore, the antibacterial effect of LZM would be sustained after PTT so as to eliminate the residual bacteria. To create an all-in-one wound dressing that could provide a comprehensive treatment to chronic wound, we came up with the GelMA-EGF/Gelatin-MPDA-LZM bilayer hydrogel dressing. The two layers were designed to target different phase in wound healing respectively. Gelatin-containing MPDA-LZM nanoparticles formed the inner layer, which could solve the infection and inflammation caused by biofilms. Gelatin possesses a thermo-reversible gel−sol transition capability[38,39], which exhibits a controlled bulk release of nanoparticles by temperature rise[40]. In this way, MPDA-LZM nanoparticles would be free to penetrate into the biofilms while PTT. The outer layer was mainly made up by gelatin methacryloyl (GelMA). Stabilized by photo-crosslinking, GelMA serves as a strong support to wound which is good for cell attachment and proliferation[30]. Besides, epidermal growth factor (EGF) was added into GelMA to promote tissue regeneration and wound re-epithelialization[41,42]. Therefore, the GelMA-EGF/Gelatin-MPDA-LZM bilayer hydrogel dressing could not only perform PTT to eradicate biofilms, but also promote the repair of chronic wounds directly by itself, which provided an innovative phased treatment to chronic wounds.

2. Materials and methods

2.1. Materials

Pluronic F-127, lysozyme from chicken egg white, 3-(4,5-Dimethylthiazol-2-yl)-2, 5-diphenyltetrazolium bromide (MTT), gelatin from porcine skin, methacrylic anhydride, and lithium phenyl-2,4,6-trimethyl benzoyl phosphinate (LAP) were purchased from Sigma−Aldrich (Missouri, USA). Dopamine hydrochloride, 1,3,5-trimethylbenzene (TMB), and crystal violet were purchased from Aladdin Co. (Shanghai, China). *Escherichia coli* (ATCC 25922), tryptone soy broth (TSB) medium, and Luria−Bertani broth (LB) medium were obtained from HuanKai Microbial (Guangzhou, China). Murine epidermal growth factor (EGF) was obtained from Pepro Tech (New Jersey, USA).

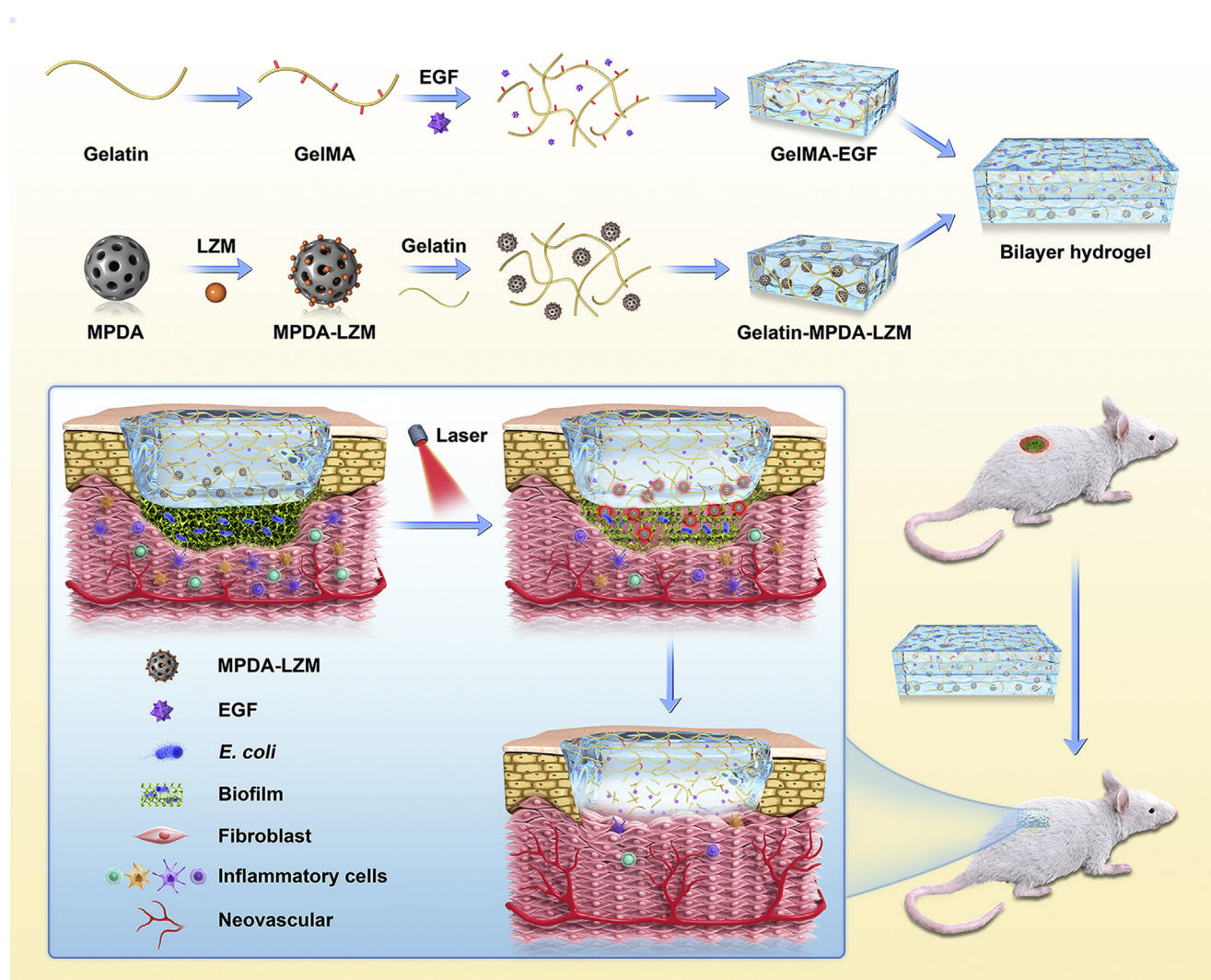### 2.2. Synthesis of MPDA-LZM nanoparticles

MPDA nanoparticles were synthesized as previous description[32]. Briefly, 0.15 g dopamine hydrochloride and 0.1 g surfactant F-127 were added to mixed solvents of ethanol and water. The solution was stirred in dark for 15 min, and then, 160 μL of TMB was dropwise added under sonication. Subsequently, 375 μL of ammonia water was added to the solution. After stirring for 2 h, the solution was centrifuged (13 000 rpm, 10 min) by a centrifuge (Thermo Scientific MICRO 17, Waltham, USA) and the sediment was collected. MPDA nanoparticles were obtained after washing by ethanol and ultrapure water.

MPDA-LZM nanoparticles were synthesized by a one-step process. MPDA nanoparticles and LZM were mixed (1:1) in ultrapure water and stirred for 24 h. The sediment after centrifugation was collected and resuspended for further use.

2.3. Characterizations of MPDA-LZM nanoparticles

The morphology and size of nanoparticles were observed by scanning electron microscopy (SEM, FEI Quanta 400FEG, USA). Additionally, the porosity of nanoparticles was characterized by specific surface area and porosity analyzer (Micromeritics, Atlanta, USA). The LZM loading capacity of MPDA-LZM nanoparticles was quantified by BCA Protein Assay Kit (Beyotime P0012, Shanghai, China). The hydrodynamic size and zeta potential of nanoparticles were measured using a Malvern Zetasizer (Malvern Nano ZS90, UK).

Scheme 1   The preparation process of GelMA-EGF/Gelatin-MPDA-LZM bilayer hydrogel dressing and its application on chronic wound.

2.4. Photothermal performance study of MPDA-LZM nanoparticles

To study the photothermal performance of MPDA-LZM nanoparticles, various concentrations (50, 100, 200, and 400 μg/mL) of MPDA-LZM nanoparticles solutions were irradiated by an 808 nm laser (BWT Beijing Ltd., Beijing, China) with different power densities (0.5, 1.0, and 1.5 W/cm^2) for 10 min. The real-time temperature of different solutions was monitored and recorded by using a digital thermometer with a thermocouple probe. The photothermal stability of MPDA-LZM nanoparticles was evaluated by on/off cycles. Briefly, MPDA-LZM nanoparticles solution (200 μg/mL) was irradiated by 808 nm laser at 1.0 W/cm^2 for 15 min to reach a steady maximum temperature. Then the laser was switched off for another 15 min to obtained the cooling process. The whole heating-cooling process was repeated for three cycles.

2.5. Antibacterial experiments in vitro

E. coli (ATCC 25922) were incubated overnight with LB culture medium and diluted to 10^8 CFU/mL. Subsequently, 100 μL of phosphate-buffered saline (PBS) or MPDA-LZM nanoparticles was added into 100 μL of E. coli suspension to reach a final concentration of 0, 100, 200, and 400 μg/mL. The mixed suspension was then irradiated with or without 808 nm laser (BWT Beijing Ltd.) at 1.0 W/cm^2 for 10 min. The viability of bacteria was corresponding to the absorbance of bacteria suspension at 600 nm measuring with a microplate reader (BioTek Synergy 4, Vermont, USA). The survival percentage of bacteria was calculated as Eq. (1), where A indicates the absorbance when irradiation time is 0 min, and B is the absorbance after irradiation.

$$\text{Survival percentage } (\%) = B/A \times 100 \tag{1}$$

2.6. Measurements of activity of lysozyme

The influence of heat on the enzymatic activity of lysozyme was measured by evaluating the corresponding antibacterial activity. Briefly, lysozyme solutions were prepared and incubated in 37, 50, and 70 °C for 2 h, respectively. Then, above lysozyme solutions were incubated with E. coli bacterial suspensions (10^6 CFU/mL) at 37 °C for 1 h. The absorbance of bacterial suspensions at OD_{600} before and after incubation was measured by microplate reader (BioTek). The relative activity of lysozyme was measured as Eq. (2), where C is the antibacterial ratio in the control group and D is the antibacterial ratio in the experimental group.

$$\text{Relative activity } (\%) = D/C \times 100 \tag{2}$$

2.7. Cytocompatibility evaluation in vitro

Mouse fibroblasts (NIH-3T3) were used in cytocompatibility evaluation in vitro. NIH-3T3 cells were first seeded into 96-well plates (3×10^3 cells per well) and incubated for 24 h at 37 °C with 5% CO$_2$. After that, different concentrations (25, 50, 100, 200, and 400 μg/mL) of MPDA-LZM nanoparticles were co-incubated with NIH-3T3 cells for another 24 h. After co-incubation, the culture medium was removed and the treated cells were washed with PBS for three times. The standard MTT assays were performed to measure the relative cell viability. Briefly, 100 μL of fresh culture medium and 20 μL of MTT solution (5 mg/mL) was added in the 96-well plates. All the liquid was removed after incubation for 4 h at 37 °C. One hundred microliter of DMSO was added each well and the 96-well plates was placed in a shaker for 20 min. The relative cell viability was determined by measuring the absorbance of the corresponding supernatant at 490 nm with a microplate reader (BioTek).

2.8. Preparation of GelMA-EGF/gelatin-MPDA-LZM hydrogel

GelMA was prepared as reported previously[43,44]. Briefly, gelatin was dissolved in PBS at 50 °C with a concentration of 10% (w/v). Then, methacrylic anhydride was dropwise added into gelatin solution under stirring to make a final concentration of 16% (v/v). After 3 h reaction, four-fold volume of PBS was added to the solution to terminate the reaction. The solution was next dialyzed for 6 days followed by 3 days lyophilization. The lyophilized GelMA was dissolved in PBS [15% (w/v)] containing 0.25% (w/v) of the photo-initiator lithium phenyl−2, 4, 6−trimethyl benzoyl phosphinate (LAP). Moreover, 1 μg/mL epidermal growth factor (EGF) was added to make GelMA-EGF solution. Meanwhile, 10% (w/v) gelatin solution was prepared and different concentrations of MPDA-LZM nanoparticles was dispersed in the solution for following use.

To prepare the GelMA-EGF/Gelatin-MPDA-LZM bilayer hydrogel, GelMA-EGF solution was first added into a mold and irradiated with a 405 nm light source (Sunp Biotech, Beijing, China) for 1 min. After the gelling, gelatin solution with different concentrations of MPDA-LZM nanoparticles was put upon GelMA-EGF and frozen in 4 °C for 10 min to form the bilayer hydrogel.

2.9. Characterization of GelMA-EGF/gelatin-MPDA-LZM hydrogel

The modification of methacrylic anhydride was proved by proton nuclear magnetic resonance (^{1}H NMR). GelMA and gelatin samples were dissolved in deuterium oxide to get ^{1}H NMR spectra respectively. The swelling ratio (SR) of GelMA-EGF hydrogel was measured. GelMA-EGF hydrogel with thickness of 2 mm and diameter of 10 mm was prepared by using a mold and then immersed in PBS at 37 °C for 24 h. After that, the liquid was removed and the weight of GelMA-EGF hydrogel was recorded (W_s). Next, hydrogel was lyophilized and weighed (W_d). The SR of GelMA-EGF hydrogel was determined as shown in Eq. (3).

$$SR = (W_s - W_d)/W_d. \tag{3}$$

The mechanical property of GelMA-EGF hydrogel was characterized by testing the compressive modulus. Hydrogel samples were prepared in a mold (height = 4 mm, diameter = 12 mm). The measurement of compressive stress−strain was performed by a universal tester (MTS CMT6103, USA). The rate of compressive strain was 1 mm/min and the strain level was 75%. Compressive modulus was calculated as the slope of the linear region of the stress−stain curves between 0 and 10% strain range. Rheological properties of hydrogel were measured by rheometer (HAAKE MARS III, USA). The degradation behavior of hydrogel was measured by placing GelMA-EGF hydrogel in PBS at 37 °C for 14 days and the weight of hydrogel was taken at the set time points (0, 1, 2, 4, 7, 14 days).

The morphology of hydrogel was observed by scanning electron microscopy (SEM, FEI). GelMA/Gelatin hydrogel and GelMA-EGF/Gelatin-MPDA-LZM hydrogel were prepared and lyophilized. Then, the samples were coated with gold and observed by SEM. The release behaviors of MPDA-LZM nanoparticles and EGF from hydrogel were measured. Briefly, hydrogel was placed in 3 mL of PBS and incubated at 37°C. At the set time intervals, 0.2 mL of the release medium was taken followed by the addition of 0.2 mL fresh PBS. The content of nanoparticles was measured at OD_{808} by microplate reader (BioTek). The cumulative release amount of EGF was measured by EGF ELISA kit (QuantiCyto EMC038, Shenzhen, China).

2.10. Photothermal performance study of GelMA-EGF/gelatin-MPDA-LZM hydrogel

The photothermal performance of the integrated GelMA-EGF/Gelatin-MPDA-LZM hydrogel was measured. Briefly, GelMA-EGF/Gelatin-MPDA-LZM hydrogel with different concentrations of MPDA-LZM nanoparticles (0, 100, 200, and 400 μg/mL) were formed in 48-well plates to avoid gelatin loss while the subsequent liquefaction. And then hydrogel was irradiated by an 808 nm laser (BWT Beijing Ltd.) at 1.0 W/cm^2 for 10 min. The real-time temperature of GelMA-EGF/Gelatin-MPDA-LZM hydrogel was monitored by an infrared thermal imaging camera (Fluke Ti27, Everett, USA). Viability of NIH-3T3 cells was measured to test the biological activity of EGF. Various groups of EGF were pre-treated with different temperature (30, 40, 50, 60, and 70 °C) and then the standard MTT assays were performed as previous description.

2.11. Biofilm formation

E. coli were incubated overnight in LB medium on a shaking incubator at 37 °C. Then bacteria suspension was diluted to 10^6 CFU/mL with tryptone soy broth (TSB) medium and added into 24-well plates (1 mL per well) or 96-well plates (100 μL per well). The plates were incubated at 37 °C without shaking for 5–7 days. The medium was replaced by fresh TSB medium every 24 h. The biofilm attached on the bottom of each well could be observed when the medium was discarded after incubation.

2.12. Evaluation of NIR-triggered antibiofilm activity in vitro

To evaluate the effect of photothermal therapy and lysozyme respectively, 300 μL of PBS (control), MPDA nanoparticles, and MPDA-LZM nanoparticles were added to the formed biofilms. The biofilms with different treatments were irradiated with or without 808 nm laser (BWT Beijing Ltd.) at 1.0 W/cm^2 for 10 min.

To study the NIR-triggered antibiofilm activity of GelMA-EGF/Gelatin-MPDA-LZM hydrogel. The obtained biofilms were treated with PBS (control), Gelatin hydrogel, GelMA/Gelatin hydrogel, MPDA-LZM nanoparticles, Gelatin-MPDA-LZM hydrogel, and GelMA-EGF/Gelatin-MPDA-LZM hydrogel with or without 808 nm laser irradiation (1.0 W/cm^2) for 10 min and standing for 1 h.

2.13. Crystal violet staining

After treatments, the supernatant or hydrogel in each well was removed and the remaining biofilms were gently washed with PBS for three times. Crystal violet staining was performed to evaluate the eradication of biofilms. First, 300 μL of 0.1% crystal violet

dye was added to each well and incubated at room temperature for 15 min. Then, the plates were washed thoroughly with PBS to remove redundant crystal violet dye. Biofilms after staining were imaged by camera. At last, 200 μL of ethanol was added into each well to dissolve the crystal violet, and the corresponding absorbance of crystal violet solution at 590 nm was measured with a microplate reader (BioTek) to quantify the amounts of remaining biofilms.

2.14. Live/dead staining observation of biofilms by 3D CLSM

The viability of bacteria in biofilms was studied by live/dead staining analysis. First, *E. coli* suspension incubated overnight was diluted to 10^6 CFU/mL with tryptone soy broth (TSB) medium. 1 mL of bacteria suspension was added into confocal dish with a glass bottom and incubated at 37 °C without shaking for 5–7 days to form biofilms. The medium was discarded after the formation of biofilms. PBS (control), GelMA-EGF/Gelatin hydrogel, and GelMA-EGF/Gelatin-MPDA-LZM hydrogel were placed onto the surface of biofilms respectively and irradiated with or without 808 nm laser (BWT Beijing Ltd.) at 1.0 W/cm^2 for 10 min and standing for 1 h. The remaining biofilms were gently washed with PBS for three times after the supernatant or hydrogel was removed. SYTO 9/PI Live/Dead bacterial viability kit (Thermo Fisher L7012, Waltham, USA) was used by following corresponding instruction manual. SYTO 9 and PI were equally mixed and diluted with TSB medium before added on top of the remaining biofilms. Then the confocal dishes were incubated for 15 min in dark. After incubation, the biofilms were examined and imaged by a 3D confocal laser scanning microscope (CLSM, Olympus FV3000, Tokyo, Japan).

2.15. Mouse cutaneous wound infection model

All animal experiments were approved by Institutional Animal Care and Use Committee of Sun Yat-sen University. Six-week-old female BALB/c mice were obtained from Guangdong Medical Laboratory Animal Center. The mice were randomly divided into six groups as follows: control, GelMA/Gelatin hydrogel + laser, GelMA-EGF/Gelatin hydrogel + laser, GelMA/Gelatin-MPDA-LZM hydrogel + laser, GelMA-EGF/Gelatin-MPDA-LZM hydrogel + laser, and GelMA-EGF/Gelatin-MPDA-LZM hydrogel. First, the mouse was anesthetized and hair on dorsal side of the mouse was shaved. A circular wound with a diameter of about 10 mm was made on the dorsum of each mouse. Subsequently, 100 μL of *E. coli* suspension (10^8 CFU/mL) was injected to the wound and kept for 2 days to form mouse cutaneous wound infection model.

2.16. In vivo treatment of infected chronic wound

After the formation of wound infection model, experimental groups of infected wounds were treated with corresponding hydrogel dressing as above mentioned. NIR laser groups were then irradiated with an 808 nm laser (BWT Beijing Ltd.) at 1.0 W/cm^2 for 10 min. The real-time temperature on mouse wound area was monitored by an infrared thermal imaging camera (Fluke). The condition of infected wound was observed and photographed at regular time intervals.

To evaluate the photothermal therapeutic effect on *in vivo* biofilm eradication of GelMA-EGF/Gelatin-MPDA-LZM hydrogel, a standard plate counting assay was performed to obtain the

bacterial counts of the wound on Day 4. Briefly, the infected wound tissue was excised and placed into sterile PBS. After homodisperse, the solution was serially diluted to spread plate so as to count the number of bacteria. The photographs of bacterial colony plates were taken at 10^3 times dilution. The survival rate of bacteria was calculated as Eq. (4):

$$\text{Survival rate} = N/N_c \quad (4)$$

where N represented the CFU number of different treated group, and N_c was the CFU number of control group. Besides, to observe the eradication of biofilms more directly, wound area skin tissues were obtained before and after PTT. After fixed with 4% para-formaldehyde solution and gradually dehydrated in 30, 50, 70, 90%, and absolute ethanol solutions, the samples were observed by scanning electron microscopy (SEM, FEI).

After 12 days treatment, the mice were euthanized. The skin tissues of infected wound were obtained and fixed with 4% paraformaldehyde solution. Subsequently, the tissues were embedded in paraffin and sliced. H&E staining and Masson's trichrome staining were performed to evaluate the condition of wound healing. In the meantime, Giemsa staining was performed to detect the condition of bacterial infection in wound. Moreover, cell proliferation of wound tissue was evaluated by Ki-67 immunohistochemical staining. To further assess the efficacy of the hydrogel dressing, angiogenesis in wound area was evaluated by immunofluorescence staining of CD31 and α-SMA.

Additionally, H&E staining of major organs including heart, liver, spleen, lung, and kidney was conducted to evaluate the *in vivo* biosafety of GelMA-EGF/Gelatin-MPDA-LZM hydrogel dressing.

2.17. Statistical analysis

Quantitative data were presented as means $\pm$ SD of at least three samples and analyzed by one-way analysis of variance (ANOVA) and Student's t-test. Values of $^*P < 0.05$, $^{**}P < 0.01$, and $^{***}P < 0.001$ were considered as statistically significant.

3. Results and discussion

3.1. Preparation and characterization of MPDA-LZM nanoparticles

MPDA-LZM nanoparticles were the major component of biofilms eradication in GelMA-EGF/Gelatin-MPDA-LZM bilayer hydrogel. To prepare MPDA-LZM nanoparticles, MPDA nanoparticles were first synthesized by dopamine polymerization, LZM was then loaded through electrostatic interaction. After loading of LZM, the distinction on morphology between two kinds of nanoparticles was observed. The SEM images (Fig. 1A and B) displayed uniform spherical structure of MPDA nanoparticles with diameter around 300 nm, and the mesoporous was clearly distributed. While MPDA-LZM nanoparticles had larger diameter (about 300 nm), mesoporous structure was not obviously to observe. The measured hydrodynamic size of MPDA-LZM nanoparticles was 394 nm, slightly larger than that of MPDA nanoparticles (346 nm). Supporting Information Fig. S1B showed that zeta potentials of MPDA, LZM, and MPDA-LZM were −17.63, 22.87, and 9.60 mV, respectively, indicating the negative charge of MPDA was neutralized after the electrostatic attraction of positively charged LZM. Furthermore, the porosity

of MPDA nanoparticles was characterized in Supporting Information Fig. S1C and D. MPDA nanoparticles possessed BET surface area of 28.08 m^2/g and approximate pore diameter of 9.32 nm, exhibiting great potential of drug loading. Consequently, the proper LZM loading capacity was 18.00 $\pm$ 1.37% *via* quantitative analysis.

The photothermal performance of MPDA-LZM nanoparticles was comprehensively evaluated. As shown in Fig. 1C, MPDA-LZM nanoparticles displayed concentration-dependent temperature change under 808 nm NIR laser in 10 min. Specifically, the temperature rapidly increased from 25.0 to 48.7 and 59.8 °C at a concentration of 200 and 400 µg/mL, respectively. Additionally, the maximum temperature (Fig. 1D) of 200 µg/mL MPDA-LZM nanoparticles solution at various power densities (0.5, 1.0, and 1.5 W/cm^2) increased to 37.8, 48.7, and 54.0 °C within 10 min irradiation, respectively. Moreover, the excellent photothermal stability of MPDA-LZM nanoparticles were demonstrated in Fig. 1E. The recycling temperature variations of 200 µg/mL of MPDA-LZM nanoparticles were recorded under 808 nm NIR laser radiation for 15 min (laser on), followed by natural cooling to room temperature for 15 min (laser off) for three laser on/off cycles. The maximum temperature of MPDA-LZM nanoparticles exhibited no significant deterioration during three on/off cycles which highly demonstrated the excellent stability of photothermal performance of MPDA-LZM nanoparticles. In our whole bilayer GelMA-EGF/Gelatin-MPDA-LZM hydrogel system, MPDA-LZM nanoparticles would be dispersed homogeneously in gelatin layer to achieve light activatable drug release and photothermal therapy simultaneously. It's important to make sure that gelatin makes no differences on the photothermal performance of MPDA-LZM nanoparticles. So, we next measured the temperature changes of MPDA-LZM nanoparticles in gelatin solution under 808 nm NIR laser in 10 min (Fig. 1F). It was clear that dispersed in gelatin had no influences on the photothermal property of nanoparticles.

3.2. In vitro antibacterial activity of MPDA-LZM nanoparticles

The antibacterial activity of MPDA-LZM nanoparticles were investigated against *E. coli*. As shown in Supporting Information Fig. S2A, there are no significant differences on the bacterial survival of 100 µg/mL MPDA-LZM nanoparticles-treated group whether with or without 808 nm NIR laser radiation comparing with control group. However, the bacterial survival percentage was obvious decreased to 77.42% and 46.78% in 200 and 400 µg/mL MPDA-LZM nanoparticles-treated groups, respectively. The concentration-dependent decrease of bacterial survival percentage indicated the effective antibacterial ability of MPDA-LZM nanoparticles. Higher concentration of MPDA-LZM nanoparticles exhibited better antibacterial ability.

Besides, the influence of heat on the activity of lysozyme was evaluated. It was reported that the activity of lysozyme remained stable between 25 and 60 °C[37]. To further confirm that, the prepared lysozyme solutions were first incubated in 37, 50 and 70 °C for 2 h, and then the relative activities were measured (Fig. S2B). Obviously, the relative activities of lysozyme had no significant differences between 37 °C group and 50 °C group. When the incubation temperature was 70 °C, there was a slight decrease of lysozyme activity. Therefore, a low temperature photothermal therapy around 50 °C would not interfere the relative activities of the lysozyme loaded on MPDA nanoparticles.
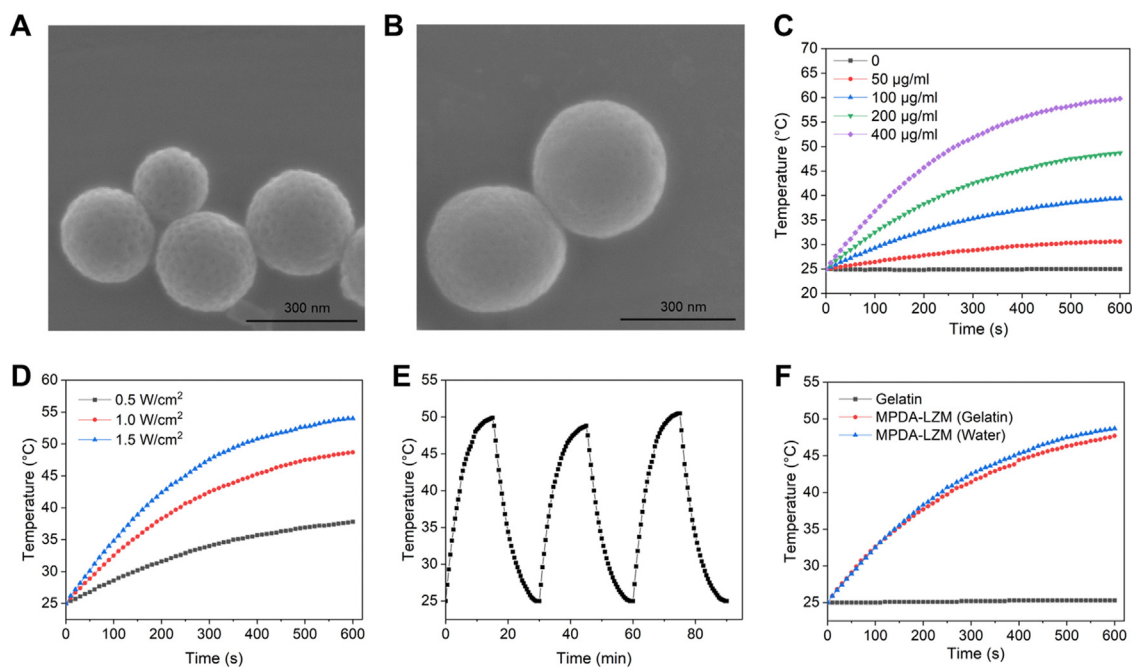
Figure 1 The morphology and photothermal performance of MPDA-LZM nanoparticles. (A, B) SEM images of (A) MPDA nanoparticles and (B) MPDA-LZM nanoparticles (scale bar: 300 nm). (C) Temperature change of MPDA-LZM nanoparticles with NIR irradiation (1.0 W/cm^2) at different concentrations. (D) Temperature change of MPDA-LZM nanoparticles (200 μg/mL) with NIR irradiation (0.5, 1.0, and1.5 W/cm^2). (E) Recycling heating profiles of MPDA-LZM nanoparticles (200 μg/mL) with NIR irradiation (1.0 W/cm^2) for three on/off cycles. (F) Temperature change of MPDA-LZM nanoparticles (200 μg/mL) with NIR irradiation (1.0 W/cm^2) in different solvents.

### 3.3. In vitro cytocompatibility assay of MPDA-LZM nanoparticles

The cytocompatibility of nanomaterials is quite important in biomedicine. Therefore, we assessed the cytocompatibility of MPDA-LZM nanoparticles by incubating fibroblasts (NIH-3T3) with various concentrations of MPDA-LZM nanoparticles for 24 h. The cell viability of NIH-3T3 cells was shown in Supporting Information Fig. S3. Compared with control group, the cell viability maintained nearly 100% when the concentration of nanoparticles ranged from 25 to 200 μg/mL. Though there was a slight decrease when the concentration was up to 400 μg/mL, the cell viability was still above 85% which means it had no significant effect on proliferation of NIH-3T3. Generally, the result indicates that MPDA-LZM nanoparticles has an excellent cytocompatibility.

Taking an overall consideration of all the results in Figs. 1, S2, and S3, a concentration of 200 μg/mL of MPDA-LZM nanoparticles was chosen for the subsequent application on experiments. It could reach an expectation of effective antibacterial activity meanwhile with enough photothermal performance and cytocompatibility as we need.

3.4. Lysozyme-enhanced photothermal effect to eradicate biofilms

In our design, the lysozyme-enhanced PTT for biofilms eradication would be achieved totally by MPDA-LZM nanoparticles. To figure out the antibacterial effect of MPDA-LZM nanoparticles and the synergistic effect between photothermal therapy and lysozyme, we added MPDA nanoparticles and MPDA-LZM nanoparticles to the in vitro established biofilms respectively. Fig. 2 showed the crystal violet staining image of treated biofilms and corresponding absorbance at OD$_{590}$. Compared with control group, biofilms were nearly completely eradicated by MPDA-LZM nanoparticles with laser irradiation. The result demonstrated the excellent biofilm eradication capability of MPDA-LZM nanoparticles. For comparison, MPDA nanoparticles with laser only performed photothermal effect to biofilms. The residual biofilm mass in MPDA nanoparticles-treated group indicated that common photothermal therapy was effective to biofilms eradication but not good as the effect combined with lysozyme. Furthermore, biofilms treated with MPDA-LZM nanoparticles without laser irradiation showed slight damage, which means lysozyme can hardly destroy biofilms without the assistance of photothermal effect. As we referred before, EPS of biofilms was as firm as a physical barrier that could obstruct the penetration of normal antibacterial agents. We hypothesized that the antibacterial effect of MPDA-LZM nanoparticles without laser irradiation was limited because LZM alone could hardly penetrate into biofilms and kill the bacteria inside it. However, when the structure of biofilms was incompact under the physical destruction of PTT, LZM could be released to bacteria and exert its best antibacterial capability by hydrolyze bacterial cell wall. All of these results proved that there is a synergistic effect between photothermal therapy and lysozyme on biofilms eradication. And the lysozyme-enhanced photothermal therapy shows sufficient destruction of biofilms.
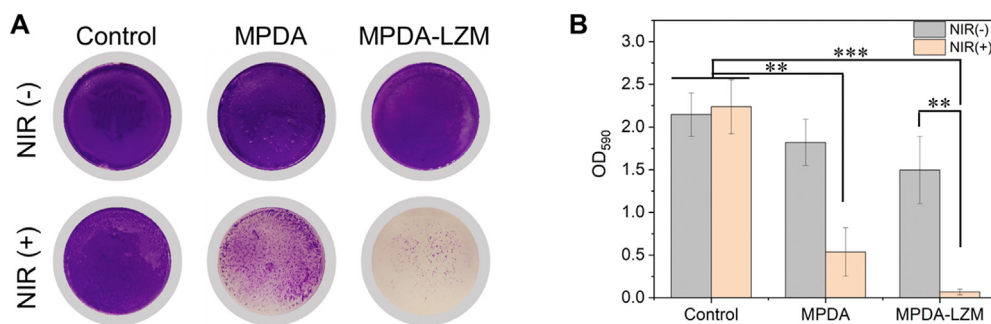
Figure 2 Lysozyme-enhanced PTT effect on biofilm eradication. (A) Photographs of crystal violet stained *E. coli* biofilms treated with PBS, MPDA nanoparticles, MPDA-LZM nanoparticles with or without NIR irradiation and (B) corresponding absorbance at 590 nm ($n = 3$, **$P < 0.01$, ***$P < 0.001$).

3.5. Preparation and characterization of GelMA-EGF/gelatin-MPDA-LZM hydrogel

As a major component of GelMA-EGF/Gelatin-MPDA-LZM bilayer hydrogel, GelMA was synthesized first. The ^{1}H NMR spectra (Supporting Information Fig. S4) showed that meth-acrylic anhydride was successfully modified to gelatin. The characteristic peaks at 5.3 and 5.6 ppm indicated that gelatin was converted to GelMA. Next, different concentrations [5%, 10%, 15%, and 20% (*w/v*)] of GelMA were prepared to test the capability of photo-crosslinking. As shown in Supporting Information Fig. S5A, all concentrations of GelMA solution transformed to gel phase after exposed in 405 nm for 1 min. The photo-crosslinking of GelMA was irreversible because it couldn't turn back to solution phase in 37 °C like gelatin did. Moreover, adding EGF into GelMA had no effect on the photo-crosslinking ability of GelMA (Fig. 3A). The swelling and mechanical property of GelMA-EGF hydrogel were measured subsequently. Supporting Information Fig. S6 showed that swelling ratio of GelMA-EGF hydrogel gradually decreased while the concentration of GelMA increasing from 5% to 20% (*w/v*). However, compressive stress−strain curves (Supporting Information Fig. S7) showed an ascending tendency of mechanical property with concentration increasing. The compressive modulus had a remarkable increase from 27.63 ± 1.79 to 131.87 ± 5.87 kPa, demonstrated that GelMA-EGF hydrogel became stiffer when the concentration of GelMA increased to 20% (*w/v*). In a comprehensive consideration of all the characteristics, 15% (*w/v*) was an optimal concentration of GelMA-EGF hydrogel. It possessed an appropriate swellability to absorb exudate and a compressive modulus of 95.07 ± 8.43 kPa that could provide strong support like native dermis[30]. Besides, the thermo-reversible gel−sol transition behavior of gelatin was verified in Fig. S5B and Fig. 3B. A concentration of 10% (*w/v*) was chosen for further study because its great thermo-reversible behavior with expectant strength in gel phase and fluidity in solution phase. The mix of MPDA-LZM nanoparticles didn't influence the thermo-reversible behavior of gelatin either (Fig. 3B). We next measured the rheological properties of different hydrogel. The temperature-dependent curves of storage modulus (G′) and loss modulus (G″) (Supporting Information Fig. S8A) showed clearly that the gelation temperatures of GelMA-EGF hydrogel and Gelatin-MPDA-LZM hydrogel were both between 25 and 30 °C, consistent with their actual performance previously. Since the GelMA-EGF hydrogel would not

revert to solution phase at 37 °C because of the irreversible photo-crosslinking, its degradation behavior at 37 °C was measured *in vitro*. The results in Fig. S8B demonstrated the remaining ratio of GelMA-EGF hydrogel was still above 80% after placed in PBS at 37 °C for 14 days, indicating its long term retention for wound healing application.

The morphology of GelMA/Gelatin hydrogel and GelMA-EGF/Gelatin-MPDA-LZM hydrogel was observed by SEM. In Fig. 3C−F, both layer of the two kinds of hydrogel displayed porous structure. The addition of EGF did not make a difference to the microstructure of GelMA hydrogel. Similarly, dispersed MPDA-LZM nanoparticles in gelatin didn't change the microstructure of gelatin. Demonstrated the potential use of GelMA/Gelatin-based bilayer hydrogel on loading macromolecule or nanocomposite. We then measured the release behaviors of MPDA-LZM nanoparticles and EGF from GelMA-EGF/Gelatin-MPDA-LZM hydrogel. The release curves were demonstrated in Supporting Information Fig. S9, MPDA-LZM nanoparticles achieved bulk release under the irradiation of 808 nm laser within 2 min, which was attributed to the rapid gel−sol transition of gelatin. Differently, EGF exhibited a slow cumulative release of about 55% after 7 days.

The photothermal performance of the integrated GelMA-EGF/Gelatin-MPDA-LZM bilayer hydrogel was studied. As the photographs in Fig. 3G and H, GelMA-EGF/Gelatin-MPDA-LZM bilayer hydrogel was put onto filter paper and irradiated with 808 nm laser. We could find that the Gelatin-MPDA-LZM layer liquefied quickly in 2 min under laser irradiation, which would be beneficial to quick release of nanoparticles to penetrate into biofilms and exert antibacterial effect. Furthermore, GelMA-EGF layer was still strong that could protect and support the wound area. Fig. 3I and J showed the temperature change of GelMA-EGF/Gelatin-MPDA-LZM hydrogel with different concentrations of nanoparticles after irradiated for 10 min. The photothermal performance displayed similar concentration-dependent temperature change to previous nanoparticles solution, indicating the photothermal performance of MPDA-LZM nanoparticles was not impaired in the hydrogel system. The temperature of GelMA-EGF/Gelatin-MPDA-LZM hydrogel (200 μg/mL of MPDA-LZM nanoparticles) increased 22.6 °C after 10 min irradiation, which could provide sufficient photothermal effect for subsequent therapy. Besides, to figure out whether the produced heat would influence the biological activity of EGF, we tested the viability of NIH-3T3 cells treated with different temperature pre-treated EGF. Cells without EGF treatment were used as control. It
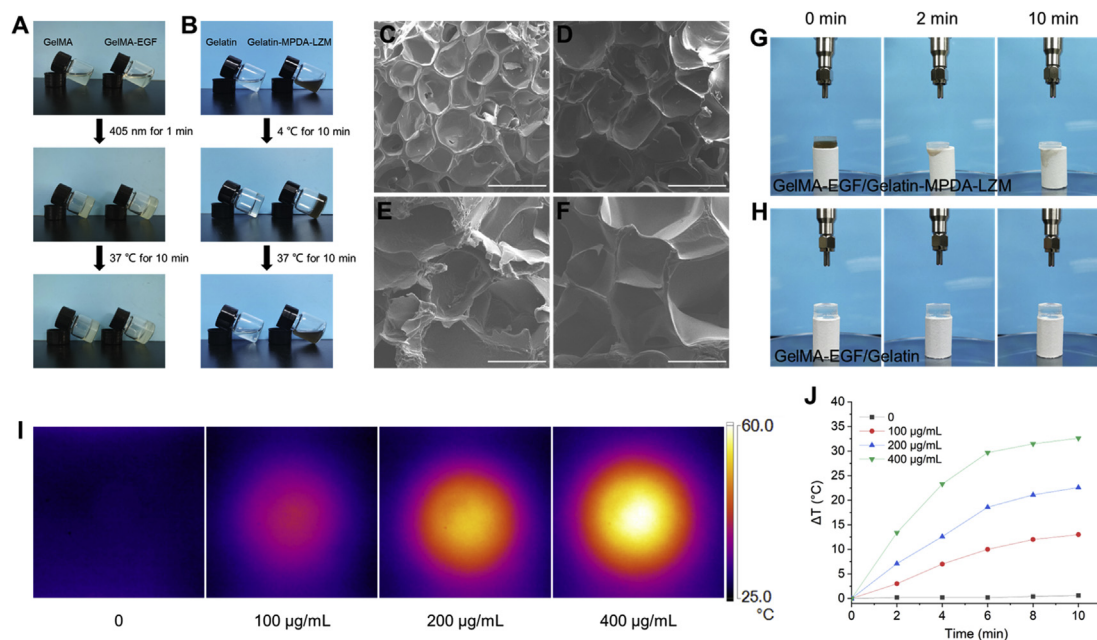
Figure 3 Characterization, microstructure, and photothermal performance of GelMA-EGF/Gelatin-MPDA-LZM bilayer hydrogel. (A) Photographs of the photo-crosslinking process of GelMA and GelMA-EGF. (B) Photographs of the thermo-reversible gel−sol transition of gelatin and Gelatin-MPDA-LZM. (C−F) SEM images of (C) GelMA, (D) GelMA-EGF, (E) Gelatin, and (F) Gelatin-MPDA-LZM hydrogel (scale bar: 500 μm). (G, H) Photographs of the liquefaction process of Gelatin-MPDA-LZM hydrogel under NIR irradiation. (I) Thermographic images of GelMA-EGF/Gelatin-MPDA-LZM hydrogel with different concentrations of nanoparticles after NIR irradiation for 10 min and (J) corresponding photothermal heating curves.

could be inferred from Supporting Information Fig. S10 that the temperature increase in hydrogel made no significant difference to the biological activity of EGF.

### 3.6. In vitro eradication of established biofilms

After a series of optimization studies, we then assessed the antibiofilm capability of GelMA-EGF/Gelatin-MPDA-LZM hydrogel on established biofilms *in vitro*. Different groups of hydrogel or nanoparticles were added onto the surface of biofilms, and PBS treatment was used as control. The results were shown in Fig. 4. Crystal violet staining could show the residual biofilms directly. We could tell from Fig. 4A and B that biofilms were obviously eradicated when MPDA-LZM nanoparticles and laser irradiation were both involved in the treatments. Indicating the excellent antibiofilm capability of GelMA-EGF/Gelatin-MPDA-LZM hydrogel. The live/dead staining assay in Fig. 4C also demonstrated that biofilms were successfully eradicated by lysozyme-enhanced photothermal therapy of GelMA-EGF/Gelatin-MPDA-LZM hydrogel. In comparison with the intact and compact biofilm structure of control group, biofilms treated with GelMA-EGF/Gelatin-MPDA-LZM hydrogel + laser exhibited a quite sparse condition in 3D CLSM images. All above results were sufficient to manifest the distinguished antibiofilm capability of GelMA-EGF/Gelatin-MPDA-LZM hydrogel.

### 3.7. In vivo therapeutic efficacy on infected wound

With the remarkable antibiofilm ability proved above, GelMA-EGF/Gelatin-MPDA-LZM bilayer hydrogel was then applied to mouse cutaneous wound infection model to verify its therapeutic efficacy. To construct the infected wound model, a full-thickness wound was made on the dorsum of BALB/c mouse. Then the wound was inoculated with *E. coli* and kept for 2 days to form infected wound with bacterial biofilms *in situ*. Different groups of bilayer hydrogel dressing were prepared and applied on mice followed with or without NIR irradiation. Fig. 5A was the representative thermographic images taken during photothermal therapeutic period. GelMA/Gelatin-MPDA-LZM hydrogel and GelMA-EGF/Gelatin-MPDA-LZM hydrogel both exhibited prominent photothermal performance under laser irradiation. The corresponding photothermal heating curves in Fig. 5B showed the temperature change of wound area in 10 min. In the two groups above mentioned, temperature of wound area went up to about 46 °C practically. The result confirmed that GelMA-EGF/Gelatin-MPDA-LZM hydrogel could perform photothermal therapy with an appropriate temperature limitation which would not injure surrounding tissues of wound.

The efficacy of lysozyme-enhanced photothermal therapy was evaluated by testing the survival rate of bacteria after therapy. Hydrogel and scar tissue upon the wound were removed after 4 days treatment which is the first timepoint of observation. As shown in Fig. 5C, apparent abscess could be observed on the wound site in groups without experiencing the process of photothermal therapy generated by MPDA-LZM nanoparticles. The existence of abscess indicated severe infected condition of the wound. And the results of standard plate counting assay were consistent with the appearance of wound sites for different treatment groups. Survival rate of bacteria (Fig. 5D) was extreme low in GelMA/Gelatin-MPDA-LZM hydrogel + laser group and GelMA-EGF/Gelatin-MPDA-LZM hydrogel + laser group, demonstrated their excellent antibacterial and antibiofilm abilities. Without laser irradiation, GelMA-EGF/Gelatin-MPDA-LZM hydrogel also exhibited antibacterial ability in some extent due to the existence of LZM, as the
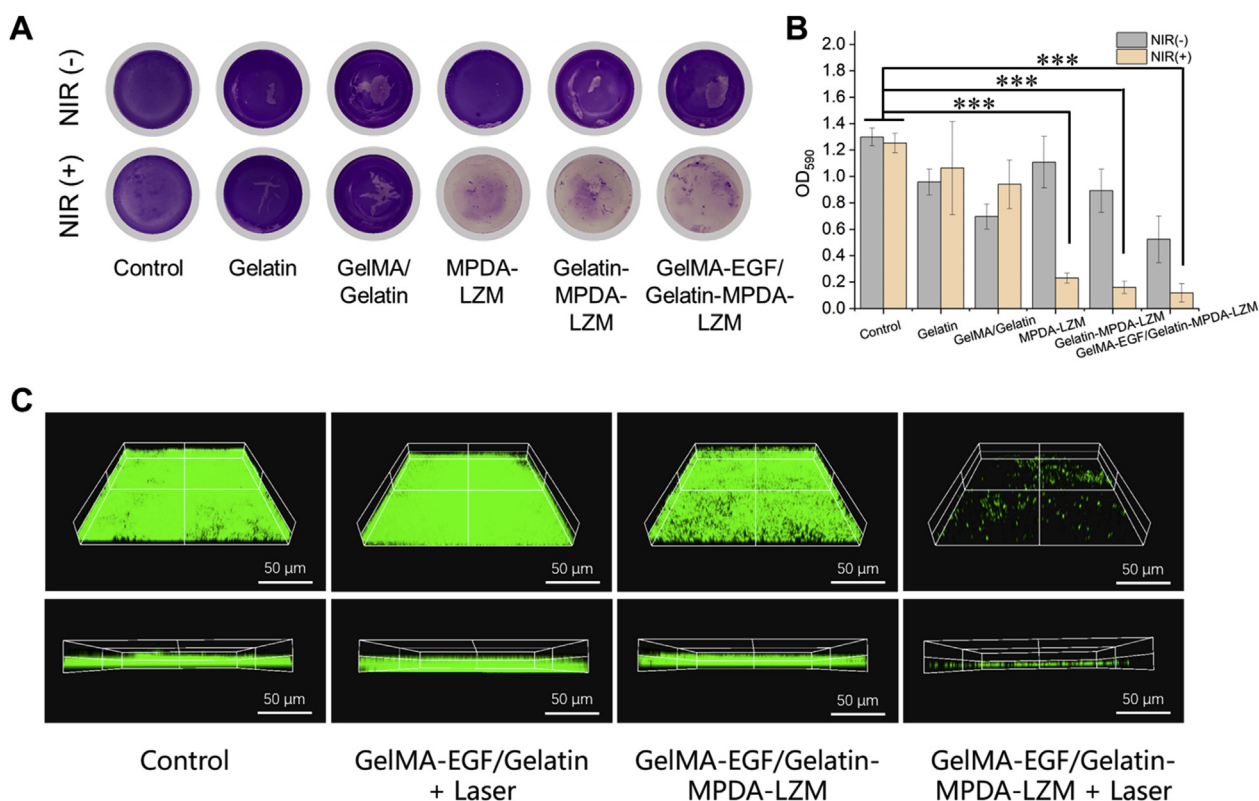
Figure 4 The capability of biofilm eradication of GelMA-EGF/Gelatin-MPDA-LZM hydrogel *in vitro*. (A) Photographs of crystal violet stained *E. coli* biofilms in different groups and (B) corresponding absorbance at 590 nm ($n = 3$, ***$P < 0.001$). (C) 3D confocal laser scanning microscopy images of SYTO 9 stained *E. coli* biofilms after different treatments (scale bar: 50 μm). The live bacteria were in green fluorescence.
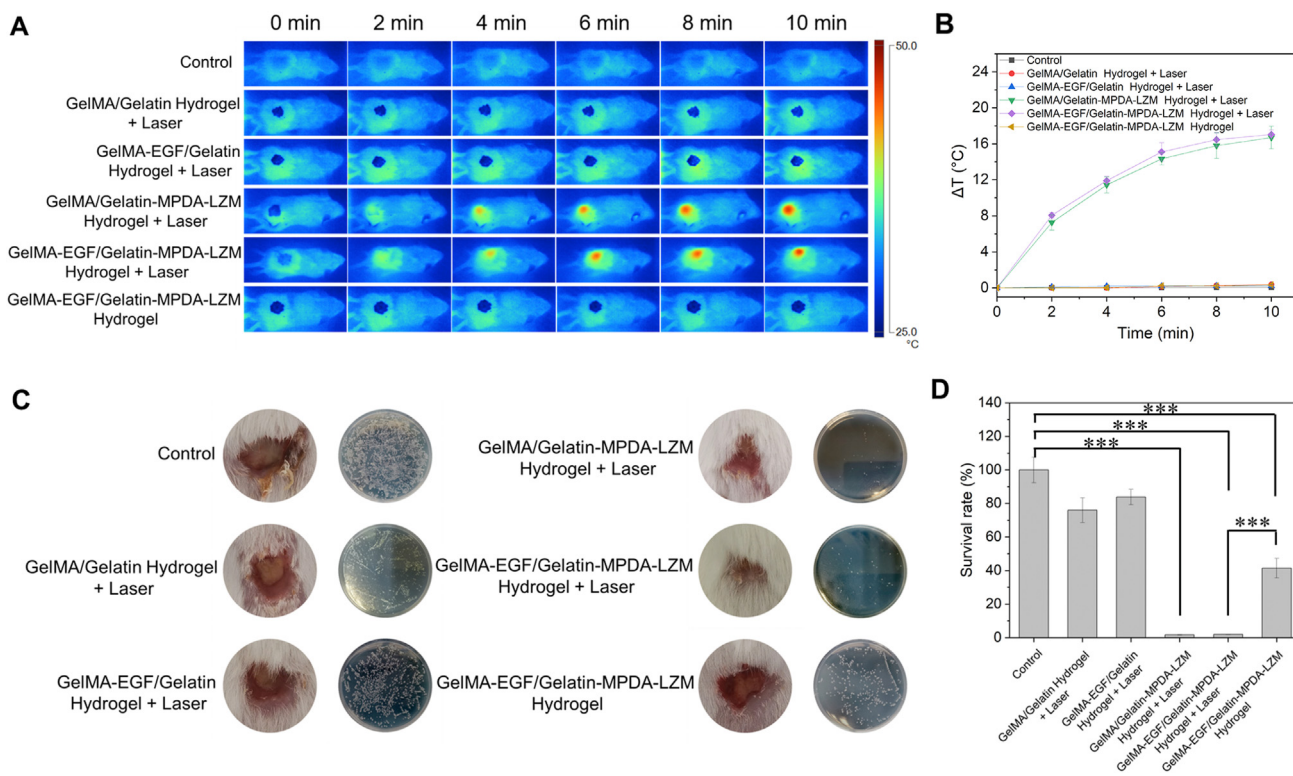
Figure 5 *In vivo* photothermal anti-infective efficacy of GelMA-EGF/Gelatin-MPDA-LZM hydrogel dressing. (A) Representative thermographic images of BALB/c mice infected wounds treated with different hydrogel systems and (B) corresponding photothermal heating curves ($n = 3$). (C, D) Representative wound photographs after treated with different hydrogel systems for 4 days and quantitative measurement of bacterial survival rate by counting CFU amounts in standard plate assay ($n = 3$, ***$P < 0.001$).
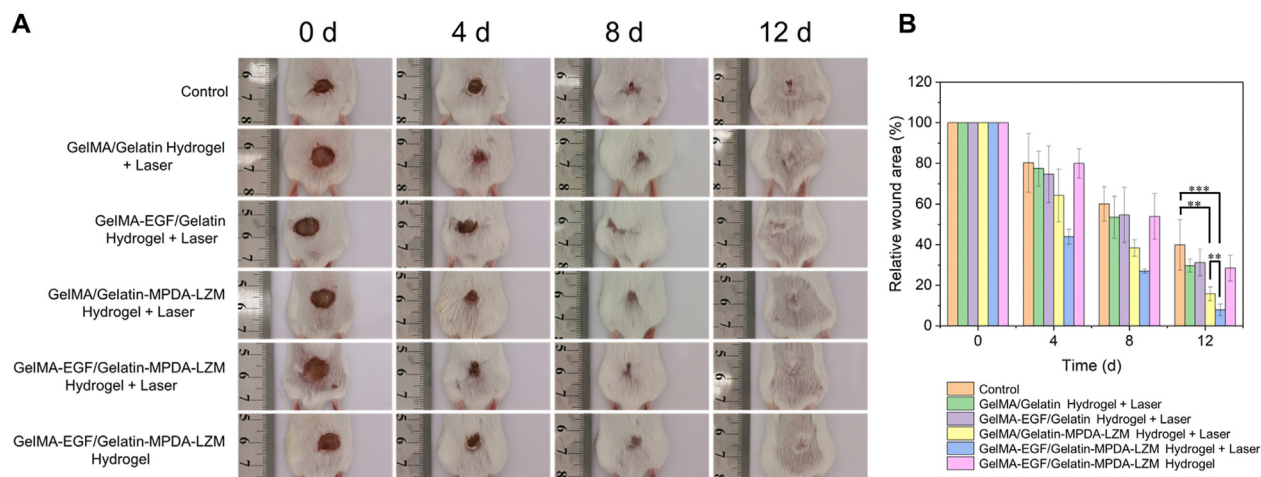
Figure 6 *In vivo* accelerated wound healing of GelMA-EGF/Gelatin-MPDA-LZM hydrogel dressing. (A) Photographs of *E. coli*-infected full-thickness dorsal cutaneous wounds of BALB/c mice treated with different hydrogel systems and (B) corresponding statistical graph of relative wound area ($n = 5$, **$P < 0.01$, ***$P < 0.001$).
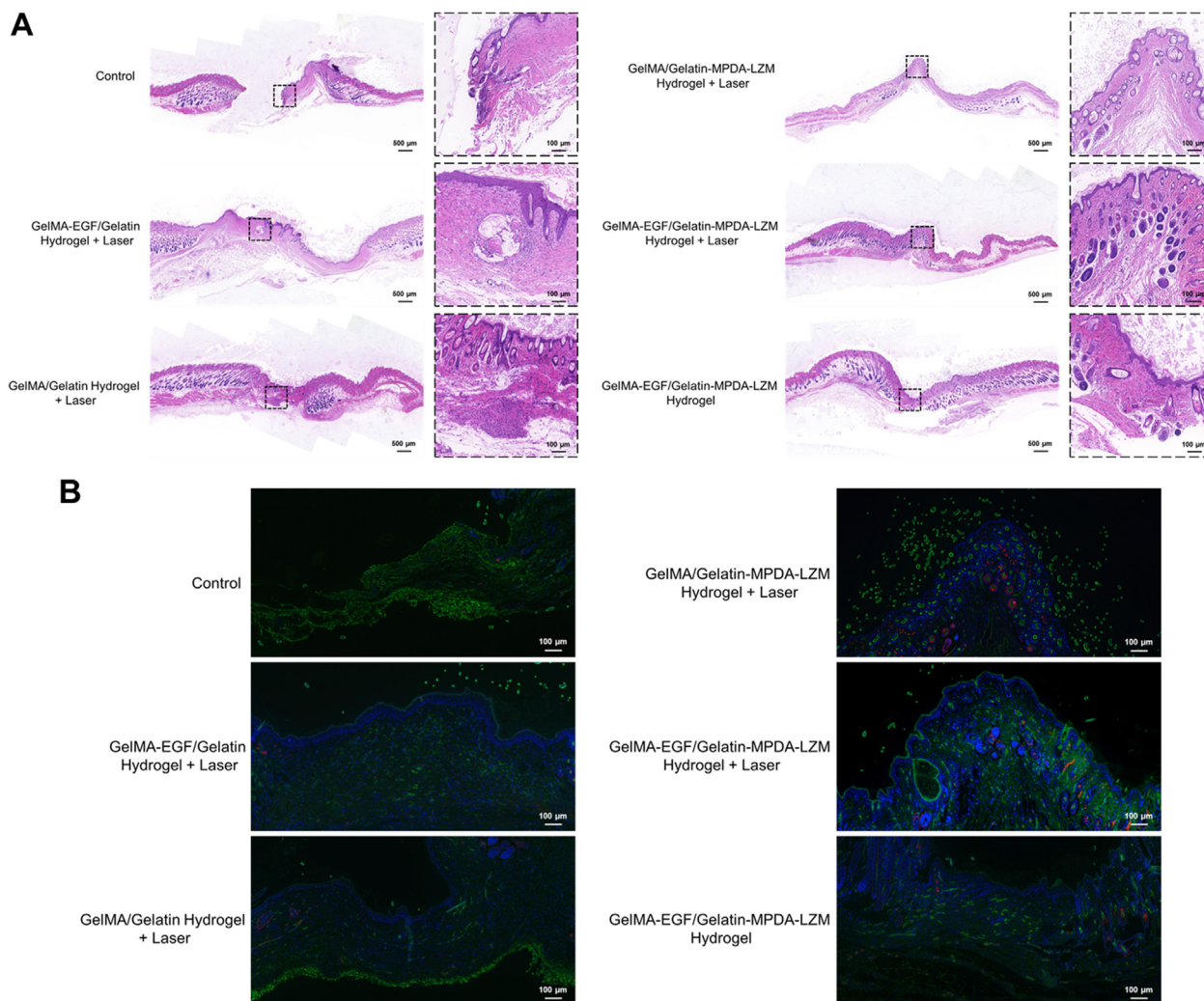
Figure 7 Histological analysis of wound tissues obtained from BALB/c mice after treatments. (A) Representative H&E staining images of wound skin tissues (scale bar: 500 μm and 100 μm for magnification). (B) Immunofluorescence images of wound skin tissues (green: CD31; red: α-SMA; scale bar: 500 μm).

survival rate of bacteria was decreased to 41.39%. But the distinction was clear when compared it with GelMA-EGF/Gelatin-MPDA-LZM hydrogel + laser group, of which the survival rate was greatly decreased to 1.92%. The results further confirmed the synergistic effect of PTT and LZM, verified the best anti-infectious efficacy of lysozyme-enhanced photothermal therapy provided by GelMA-EGF/Gelatin-MPDA-LZM hydrogel.

Photographs of wound and corresponding statistical graph of relative wound area at predetermined timepoints were shown in Fig. 6. After 12 days, the relative wound area remained at 39.89%, 29.65%, 31.21%, 15.78%, 7.90%, and 28.48% in control, GelMA/Gelatin hydrogel + laser, GelMA-EGF/Gelatin hydrogel + laser, GelMA/Gelatin-MPDA-LZM hydrogel + laser, GelMA-EGF/Gelatin-MPDA-LZM hydrogel + laser, and GelMA-EGF/Gelatin-MPDA-LZM hydrogel groups, respectively. The fastest closure rate and the smallest wound area in GelMA-EGF/Gelatin-MPDA-LZM hydrogel + laser group indicated its best therapeutic efficacy on infected wound. When compared with GelMA-EGF/Gelatin hydrogel + laser group and GelMA-EGF/Gelatin-MPDA-LZM hydrogel group, it also verified that lysozyme-enhanced photothermal therapy made a significant difference on the healing process of infected wound. Furthermore, the distinction in therapeutic efficacy of GelMA-EGF/Gelatin-MPDA-LZM hydrogel and GelMA/Gelatin-MPDA-LZM hydrogel showed that EGF contained in GelMA layer could promote the process of wound repair. However, there were no visible difference between therapeutic efficacy of GelMA/Gelatin hydrogel and GelMA-EGF/Gelatin hydrogel, demonstrated that EGF could barely exert its function without photothermal therapy performing first. In other words, the lysozyme-enhanced photothermal therapy acted predominantly in accelerating infected wound repair. Therefore, an early photothermal therapy followed by EGF promotion, provided by GelMA-EGF/Gelatin-MPDA-LZM hydrogel dressing, exhibited excellent efficacy of anti-infection and accelerating wound healing. To further prove the *in vivo* biofilm eradication effect of GelMA-EGF/Gelatin-MPDA-LZM hydrogel. Skin tissues of wound area before and after PTT were obtained and observed by SEM. As shown in Supporting Information Fig. S11, wound tissue before PTT appeared irregular structure of biofilms with numerous bacteria and EPS matrix. While the wound tissue after PTT exhibited nearly no biofilm structure, and the morphology of bacteria was damaged. The results proved that GelMA-EGF/Gelatin-MPDA-LZM hydrogel with laser irradiation could indeed eradicate biofilms and subsequently accelerated the process of wound healing *in vivo*.

3.8. Histological analysis

H&E staining of wound tissues was performed to assess the condition of wound healing. It has been shown in Fig. 7A, the wound of control group was unclosed and appeared amounts of inflammatory cells infiltration. However, the infiltration of inflammatory cells was slight
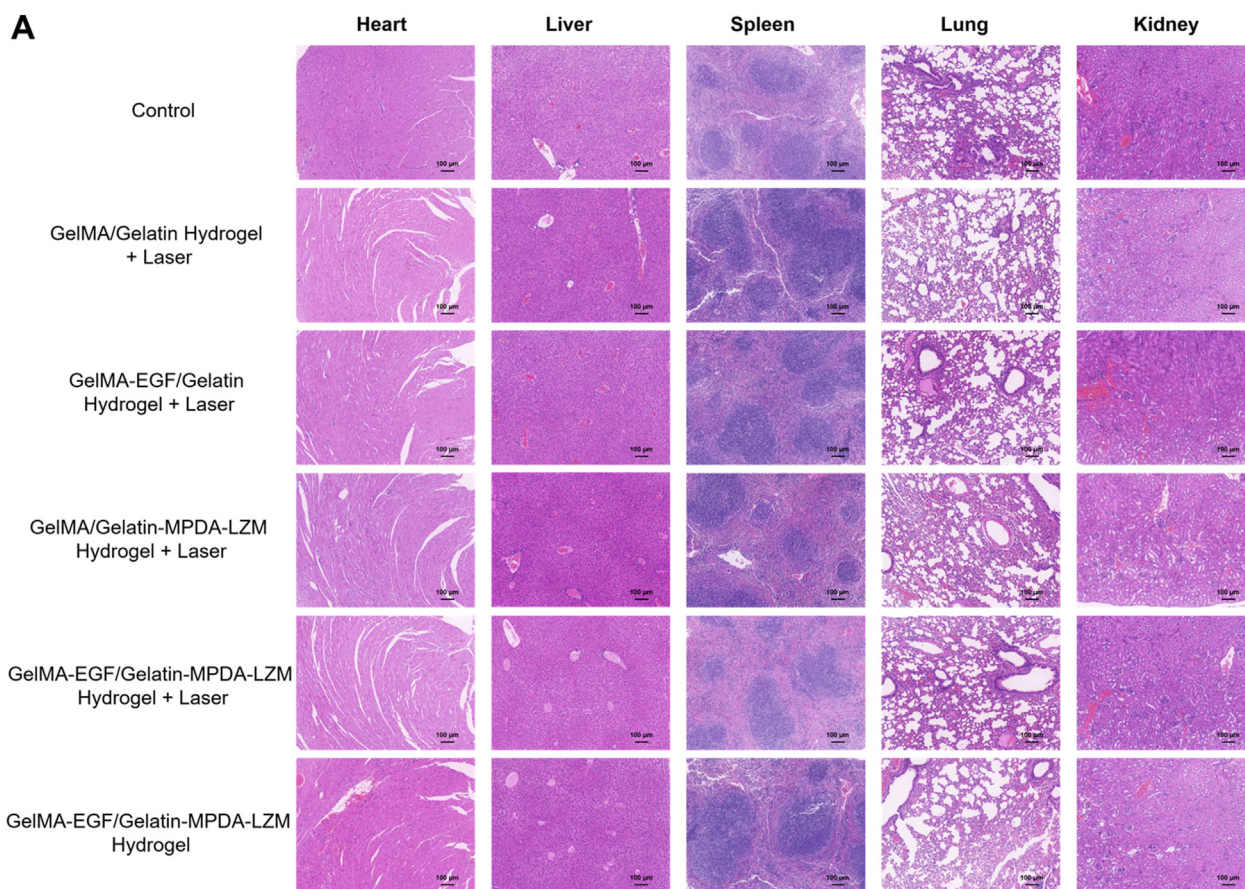
Figure 8 Biosafety assay of GelMA-EGF/Gelatin-MPDA-LZM hydrogel dressing. (A) H&E staining images of major organs obtained from mice model after 12 days' treatment (scale bar: 100 μm).

in GelMA-EGF/Gelatin-MPDA-LZM hydrogel + laser group, indicated the infection has been eliminated to a great extent and the wound healed well. The result of Masson's trichrome staining (Supporting Information Fig. S12A) was consistent with H&E staining. The situation of collagen deposition in GelMA-EGF/Gelatin-MPDA-LZM hydrogel + laser group was the thickest compared with other groups, represented its best cellular migration. Furthermore, Giemsa staining was performed to detect the bacteria in wound tissues. Fig. S12B showed clearly that the number of bacteria (red arrow) in GelMA/Gelatin-MPDA-LZM hydrogel + laser group and GelMA-EGF/Gelatin-MPDA-LZM hydrogel + laser group were relatively minor, indicated the excellent antibacterial effect of the inner layer Gelatin-MPDA-LZM hydrogel. Meanwhile, the expression of Ki-67 was increased (Fig. S12C), represented great cell proliferation of wound area in GelMA-EGF/Gelatin-MPDA-LZM hydrogel + laser group. Immunofluorescence of CD31 and α-SMA (Fig. 7B) displayed great angiogenesis condition in wound treated with GelMA-EGF/Gelatin-MPDA-LZM hydrogel + laser. The more number of vessel represented the better environment for wound repair.

Besides, the biosafety of GelMA-EGF/Gelatin-MPDA-LZM hydrogel was evaluated. H&E staining of major organs including heart, liver, spleen, lung, and kidney was performed. According to Fig. 8, there were no apparent pathologic change of the organs in all groups. The result demonstrated the great biocompatibility of our GelMA-EGF/Gelatin-MPDA-LZM bilayer hydrogel, also exhibited its potential value in clinical application.

4. Conclusions

As the increasing focus on combining biomaterials with wound healing, more and more types of functional wound dressing have been developed to greatly improve the condition of wound healing[45,46]. In this study, we presented a GelMA-EGF/Gelatin-MPDA-LZM bilayer hydrogel dressing which could effectively eradicate biofilms and promote chronic wound repair. The bilayer hydrogel dressing takes advantage of the thermo-reversible gel−sol transition capability of gelatin to achieve thermosensitive release of nanoparticles while conducting PTT. Therefore, MPDA-LZM nanoparticles could penetrate deep into biofilms and perform a lysozyme-enhanced PTT to destroy biofilms. The synergistic antibacterial effect of lysozyme and photothermal therapy was verified *in vitro*. The eradication of biofilms could improve the condition of infection and inflammatory dysregulation of chronic wound. Additionally, after the treatment to biofilms, the outer layer hydrogel remained to support and accelerate wound repair in later stage. While applying GelMA-EGF/Gelatin-MPDA-LZM bilayer hydrogel dressing to infected wound mice model, the closure rate and healing state of wound were significantly improved, further verified its remarkable efficacy. Moreover, the integrated process of treatment didn't show any apparent toxicity. In summary, our study provides an effective therapeutic strategy to solve the tough healing problem of chronic wound *via* an innovative bilayer hydrogel dressing combined with PTT, which is promising to be used clinically.

Acknowledgments

Author contributions

Bo Liu, Jie Liu, and Jie Ren designed the research. Yizhen Wang and Qijun Lv carried out the experiments and performed data analysis. You Chen, Langtao Xu and Miao Feng participated part of the experiments. Zhiyong Xiong and Jiajun Li provided experimental drugs and quality control. Yizhen Wang and Qijun Lv wrote the manuscript. Bo Liu, Jie Liu and Jie Ren revised the manuscript. All of the authors have read and approved the final manuscript.

Conflicts of interest

The authors have no conflicts of interest to declare.

Appendix A.   Supporting information

Supporting data to this article can be found online at https://doi.org/10.1016/j.apsb.2022.03.024.

References

1. Chouhan D, Dey N, Bhardwaj N, Mandal BB. Emerging and innovative approaches for wound healing and skin regeneration: current status and advances. *Biomaterials* 2019;**216**:119267.
2. Kathawala MH, Ng WL, Liu D, Naing MW, Yeong WY, Spiller KL, et al. Healing of chronic wounds: an update of recent developments and future possibilities. *Tissue Eng Part B Rev* 2019;**25**:429−44.
3. Versey Z, da Cruz Nizer WS, Russell E, Zigic S, DeZeeuw KG, Marek JE, et al. Biofilm-innate immune interface: contribution to chronic wound formation. *Front Immunol* 2021;**12**:648554.
4. Leaper D, Assadian O, Edmiston CE. Approach to chronic wound infections. *Br J Dermatol* 2015;**173**:351−8.
5. Høiby N, Bjarnsholt T, Moser C, Bassi GL, Coenye T, Donelli G, et al. ESCMID guideline for the diagnosis and treatment of biofilm infections 2014. *Clin Microbiol Infect* 2015;**21**(Suppl 1):S1−25.
6. Brackman G, Coenye T. *In vitro* and *in vivo* biofilm wound models and their application. *Adv Exp Med Biol* 2016;**897**:15−32.
7. Rodrigues M, Kosaric N, Bonham CA, Gurtner GC. Wound healing: a cellular perspective. *Physiol Rev* 2019;**99**:665−706.
8. Bjarnsholt T, Ciofu O, Molin S, Givskov M, Hoiby N. Applying insights from biofilm biology to drug development—can a new approach be developed?. *Nat Rev Drug Discov* 2013;**12**:791−808.
9. Wang J, Chen XY, Zhao Y, Yang Y, Wang W, Wu C, et al. pH-Switchable antimicrobial nanofiber networks of hydrogel eradicate biofilm and rescue stalled healing in chronic wounds. *ACS Nano* 2019;**13**:11686−97.
10. Verderosa AD, Totsika M, Fairfull-Smith KE. Bacterial biofilm eradication agents: a current review. *Front Chem* 2019;**7**:824.
11. Qiao Y, He J, Chen W, Yu Y, Li W, Du Z, et al. Light-activatable synergistic therapy of drug-resistant bacteria-infected cutaneous chronic wounds and nonhealing keratitis by cupriferous hollow nanoshells. *ACS Nano* 2020;**14**:3299−315.
12. Tong C, Zhong X, Yang Y, Liu X, Zhong G, Xiao C, et al. PB@PDA@Ag nanosystem for synergistically eradicating MRSA and accelerating diabetic wound healing assisted with laser irradiation. *Biomaterials* 2020;**243**:119936.
13. Mai B, Jia M, Liu S, Sheng Z, Li M, Gao Y, et al. Smart hydrogel-based DVDMS/bFGF nanohybrids for antibacterial phototherapy with multiple damaging sites and accelerated wound healing. *ACS Appl Mater Interfaces* 2020;**12**:10156−69.
14. Deng Q, Sun P, Zhang L, Liu Z, Wang H, Ren J, et al. Porphyrin MOF dots-based, function-adaptive nanoplatform for enhanced penetration and photodynamic eradication of bacterial biofilms. *Adv Funct Mater* 2019;**29**:1903018.

15. Hu D, Li H, Wang B, Ye Z, Lei W, Jia F, et al. Surface-adaptive gold nanoparticles with effective adherence and enhanced photothermal ablation of methicillin-resistant staphylococcus aureus biofilm. *ACS Nano* 2017;**11**:9330—9.

16. Cao C, Ge W, Yin J, Yang D, Wang W, Song X, et al. Mesoporous silica supported silver-bismuth nanoparticles as photothermal agents for skin infection synergistic antibacterial therapy. *Small* 2020;**16**: 2000436.

17. Peng H, Borg RE, Dow LP, Pruitt BL, Chen IA. Controlled phage therapy by photothermal ablation of specific bacterial species using gold nanorods targeted by chimeric phages. *Proc Natl Acad Sci U S A* 2020;**117**:1951—61.

18. Zhao B, Wang H, Dong W, Cheng S, Li H, Tan J, et al. A multifunctional platform with single-NIR-laser-triggered photothermal and NO release for synergistic therapy against multidrug-resistant gram-negative bacteria and their biofilms. *J Nanobiotechnology* 2020;**18**:59.

19. Song J, Liu H, Lei M, Tan H, Chen Z, Antoshin A, et al. Redox-channeling polydopamine-ferrocene (PDA-Fc) coating to confer context-dependent and photothermal antimicrobial activities. *ACS Appl Mater Interfaces* 2020;**12**:8915—28.

20. Yang P, Zhu F, Zhang Z, Cheng Y, Wang Z, Li Y. Stimuli-responsive polydopamine-based smart materials. *Chem Soc Rev* 2021;**50**: 8319—43.

21. Hu J, Yang L, Yang P, Jiang S, Liu X, Li Y. Polydopamine free radical scavengers. *Biomater Sci* 2020;**8**:4940—50.

22. Xie X, Tang J, Xing Y, Wang Z, Ding T, Zhang J, et al. Intervention of polydopamine assembly and adhesion on nanoscale interfaces: state-of-the-art designs and biomedical applications. *Adv Healthc Mater* 2021;**10**:2002138.

23. Liu Y, Shi L, Su L, van der Mei HC, Jutte PC, Ren Y, et al. Nano-technology-based antimicrobials and delivery systems for biofilm-infection control. *Chem Soc Rev* 2019;**48**:428—46.

24. Fulaz S, Vitale S, Quinn L, Casey E. Nanoparticle-biofilm interactions: the role of the EPS matrix. *Trends Microbiol* 2019;**27**: 915—26.

25. Yuan Z, Lin C, He Y, Tao B, Chen M, Zhang J, et al. Near-infrared light-triggered nitric-oxide-enhanced photodynamic therapy and low-temperature photothermal therapy for biofilm elimination. *ACS Nano* 2020;**14**:3546—62.

26. Li Y, Xu T, Tu Z, Dai W, Xue Y, Tang C, et al. Bioactive antibacterial silica-based nanocomposites hydrogel scaffolds with high angiogenesis for promoting diabetic wound healing and skin repair. *Theranostics* 2020;**10**:4929—43.

27. Luo Y, Wei X, Wan Y, Lin X, Wang Z, Huang P. 3D printing of hydrogel scaffolds for future application in photothermal therapy of breast cancer and tissue repair. *Acta Biomater* 2019;**92**:37—47.

28. Zhang X, Chen G, Liu Y, Sun L, Sun L, Zhao Y. Black phosphorus-loaded separable microneedles as responsive oxygen delivery carriers for wound healing. *ACS Nano* 2020;**14**:5901—8.

29. Han L, Li P, Tang P, Wang X, Zhou T, Wang K, et al. Mussel-inspired cryogels for promoting wound regeneration through photo-biostimulation, modulating inflammatory responses and suppressing bacterial invasion. *Nanoscale* 2019;**11**:15846—61.

30. Saleh B, Dhaliwal HK, Portillo-Lara R, Shirzaei Sani E, Abdi R, Amiji MM, et al. Local immunomodulation using an adhesive

hydrogel loaded with miRNA-laden nanoparticles promotes wound healing. *Small* 2019;**15**:1902232.

31. Zhu J, Wang Z, Xu X, Xu M, Yang X, Zhang C, et al. Polydopamine-encapsulated perfluorocarbon for ultrasound contrast imaging and photothermal therapy. *Mol Pharm* 2020;**17**:817—26.

32. Ding M, Miao Z, Zhang F, Liu J, Shuai X, Zha Z, et al. Catalytic rhodium (Rh)-based (mesoporous polydopamine) MPDA nanoparticles with enhanced phototherapeutic efficiency for overcoming tumor hypoxia. *Biomater Sci* 2020;**8**:4157—65.

33. Zhao X, Wang L, Gao J, Chen X, Wang K. Hyaluronic acid/lysozyme self-assembled coacervate to promote cutaneous wound healing. *Biomater Sci* 2020;**8**:1702—10.

34. Li J, Liu X, Zhou Z, Tan L, Wang X, Zheng Y, et al. Lysozyme-assisted photothermal eradication of methicillin-resistant staphylococcus aureus infection and accelerated tissue repair with natural melanosome nanostructures. *ACS Nano* 2019;**13**:11153—67.

35. Zhou D, Yang T, Qian W, Xing M, Luo G. Study of the mechanism of environmentally friendly translucent balsa-modified lysozyme dressing for facilitating wound healing. *Int J Nanomedicine* 2018;**13**: 4171—87.

36. Tan H, Jin D, Qu X, Liu H, Chen X, Yin M, et al. A PEG-lysozyme hydrogel harvests multiple functions as a fit-to-shape tissue sealant for internal-use of body. *Biomaterials* 2019;**192**:392—404.

37. Ercan D, Demirci A. Recent advances for the production and recovery methods of lysozyme. *Crit Rev Biotechnol* 2016;**36**:1078—88.

38. Ouyang L, Armstrong JPK, Chen Q, Lin Y, Stevens MM. Void-free 3D bioprinting for *in-situ* endothelialization and microfluidic perfusion. *Adv Funct Mater* 2020;**30**:1908349.

39. Yin J, Yan M, Wang Y, Fu J, Suo H. 3D bioprinting of low-concentration cell-laden gelatin methacrylate (GelMA) bioinks with a two-step cross-linking strategy. *ACS Appl Mater Interfaces* 2018;**10**: 6849—57.

40. Mir M, Ali MN, Barakullah A, Gulzar A, Arshad M, Fatima S, et al. Synthetic polymeric biomaterials for wound healing: a review. *Prog Biomater* 2018;**7**:1—21.

41. Rezaei F, Damoogh S, Reis RL, Kundu SC, Mottaghitalab F, Farokhi M. Dual drug delivery system based on pH-sensitive silk fibroin/alginate nanoparticles entrapped in PNIPAM hydrogel for treating severe infected burn wound. *Biofabrication* 2020;**13**. 015005.

42. Jiang F, Chi Z, Ding Y, Quan M, Tian Y, Shi J, et al. Wound dressing hydrogel of enteromorpha prolifera polysaccharide-polyacrylamide composite: a facile transformation of marine blooming into biomedical material. *ACS Appl Mater Interfaces* 2021;**13**:14530—42.

43. Lee J, Manoharan V, Cheung L, Lee S, Cha BH, Newman P, et al. Nanoparticle-based hybrid scaffolds for deciphering the role of multimodal cues in cardiac tissue engineering. *ACS Nano* 2019;**13**:12525—39.

44. Chen Y, Xu L, Li W, Chen W, He Q, Zhang X, et al. 3D bioprinted tumor model with extracellular matrix enhanced bioinks for nanoparticle evaluation. *Biofabrication* 2022;**14**. 025002.

45. Liang Y, He J, Guo B. Functional hydrogels as wound dressing to enhance wound healing. *ACS Nano* 2021;**15**:12687—722.

46. Li M, Liang Y, He J, Zhang H, Guo B. Two-pronged strategy of biomechanically active and biochemically multifunctional hydrogel wound dressing to accelerate wound closure and wound healing. *Chem Mater* 2020;**32**:9937—53.